Research Article

Journal of Environmental Nanotechnology

Role of pH in Modulating the Physicochemical Properties of Erbium-doped MoO_3/SiO_2 Nanoparticles

L. Jayanthi[1], P. Dhivya[2], K. Kalaivani[3] and M. Elango[1]*

[1]Department of Physics, PSG College of Arts and Science, Coimbatore, TN, India
[2]Department of Physics, EASA College of Engineering and Technology, Coimbatore, TN, India
[3]Department of Physics, Sri Krishna College of Engineering and Technology, Coimbatore, TN, India
Received: 02.08.2025 Accepted: 12.09.2025 Published: 30.09.2025
*elango@psgcas.ac.in

ABSTRACT

Molybdenum trioxide (MoO_3) coated with SiO_2 layered nanoparticles were prepared using Stöber process by wet chemical method with pH adjusted to 9, 10 and 11. The physicochemical properties of Er:MoO_3/SiO_2, such as phase confirmation, quantum confinement, surface morphology, and shape were investigated by X-ray diffraction analysis, field emission scanning electron microscopy, Raman spectroscopy, FTIR and photoluminescence spectroscopy. The vibrational behaviour of chemical bonds was analyzed by Fourier transform infrared spectroscopy. The non-stoichiometric composition and the variation in composition of as prepared samples as well as rare earth ion-doped samples were confirmed by energy dispersive X-ray analysis. The optical behaviour of the defect-related emissions varied with pH and doping with the luminescent rare earth element erbium, further illustrated the tunable nature of the optical response. This work emphasizes upconverting properties of Er-doped MoO_3/SiO_2 nanoparticles for versatile applications.

Keywords: Erbium; MoO_3/SiO_2 nanoparticles; Orthorhombic MoO_3 nanoparticles.

1. INTRODUCTION

Researchers have shown extensive interest in molybdenum trioxide (MoO_3), a wide band-gap semiconductor, owing to its remarkable physicochemical properties. It has been widely employed as a catalyst, gas sensor, photochromic and electrochromic material, and in Li-ion batteries (Yang *et al.* 2020). It has diverse oxidation states and predominantly exists in two forms. It can also occur in three polymorphic states, namely, orthorhombic α-MoO_3, hexagonal MoO_3, and monoclinic β-MoO_3, which are known to display multiphoton absorption. The multiphoton absorption is a process of strong emission of higher energy photons in the visible range when excited with lower energy infrared photons. Several host materials doped with different rare-earth ions have received special attention as stable candidates for energy conversion and storage.

MoO_3 is an attractive material due to its intense absorption near the UV region and low phonon energy. Strong polarization of MO^{3+} ion distorts the symmetry and enhances the rate of hole–electron recombination, acting as electron traps. MoO_3 clusters doped with luminescent active elements as sensitizers and Er^{3+} ions as activators have shown strong light upconversion due to efficient energy transfer from sensitizer to activator ions.

Doping may significantly affect the bandgap energy and crystalline structure. Moreover, MoO_3 has been doped with REs such Er, Yb, and Nd ions in order to study upconversion emission and find potential uses in the areas of color displays, near-infrared detectors, biological diagnostics, laser cooling, and temperature sensors (Nirmal *et al.* 2022). The surface area has increased by integration of SiO_2 matrix framework since SiO_2 is a porous material. Additionally, the chemical stability has also been increased due to SiO_2 matrix.

In this work, erbium-doped MoO_3/SiO_2 nanoparticles were prepared at varying pH (9, 10 and 11) and their physical and chemical properties were investigated.

2. SYNTHESIS PROCEURE

The nanoparticles were synthesized by Stöber process. About 1 g of cetyltrimethylammonium bromide (CTAB) was dissolved in 1:2 ratio (ethanol-to-water) and stirred continuously for half an hour. To the above solution, 0.8 mL of tetraethyl orthosilicate (TEOS) was added dropwise and stirred for 2 hours until a white precipitate was formed. The white solid was washed well with ethanol and acetone by centrifuging multiple times, and dried at 100°C for 12 hours. The obtained SiO_2 particles were preserved. To make a composite of MoO_3 and SiO_2, 0.3 g of SiO_2 particles were dissolved in 100 mL of deionized water using sonication process. Then, the precursors ammonium molybdate tetrahydrate and erbium acetate were added, followed by the slow addition of HNO_3 to the solution. Ammonia, the precipitating

agent was used to adjust the (pH 9, 10, 11) to get the desired values. At 85°C, the solution was stirred for 3 hours and left at room temperature for 4 hours to age. The collected precipitate was centrifuged and cleaned up with ethanol, acetone repeatedly and dried for 24 hours at 120°C. The dried product was calcined for 3 hours at 500°C. To understand the influence of pH and doping, the structural and functional properties of the samples were characterized.

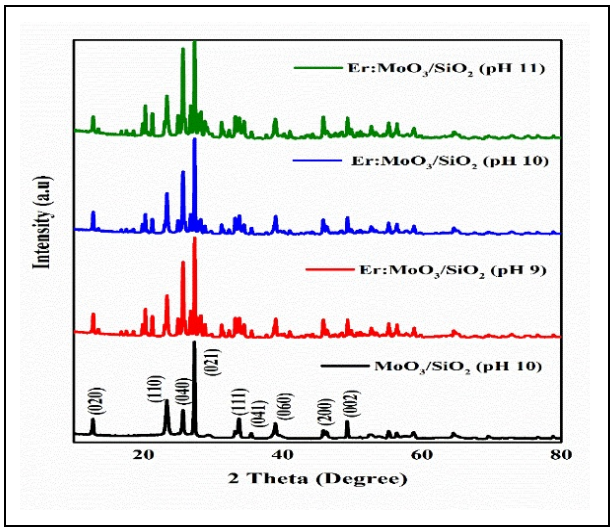


Fig. 1: XRD pattern of Er doped MoO_3/SiO_2 nanoparticles at pH 9,10 and 11

Table 1. Structural properties of Er-doped MoO_3/SiO_2 nanoparticles

Sample	Crystallite Size (nm)	Micro Strain (ε)	Stacking Fault
MoO_3SiO_2 (pH 10)	51.15	0.005233	0.003345
Er:MoO_3SiO_2 (pH 9)	43.06	0.003219	0.003031
Er:MoO_3SiO_2 (pH 10)	40.77	0.002791	0.002692
Er:MoO_3SiO_2 (pH 11)	45.25	0.006832	0.003140

3. RESULTS AND DISCUSSION

3.1 XRD Analysis

The X-ray diffraction pattern of undoped and erbium-doped MoO_3/SiO_2 samples is shown in Fig 1. The orthorhombic phase of MoO_3 well matched with the standard data (Nirmal *et al.* 2022). Further, the peak intensities of the undoped MoO_3/SiO_2 sample varied from the erbium-doped MoO_3/SiO_2 samples, and the diffraction peaks were shifted noticeably, along with new peaks. These illustrate the incorporation of Er in the host MoO_3 lattice. The intensities of major peaks such as (110), (040), (021) were observed to increase with increase in pH, which is attributed to the decrease in acidic nature of the sample. The samples prepared at pH 9 and 10 displayed sharp peaks that emphasize better crystallinity. At higher pH 11, broader peaks were observed due to the poor crystallinity and large crystallite size (Table 1). High OH^- content in pH 11 has introduced residual hydroxyl defect that led to strain-related broadening and stacking defect (Bindu and Thomas, 2014; Danks *et al.* 2016).

3.2 FTIR Spectrum

The FTIR spectrum of the sample Er-doped MoO_3/SiO_2 in Fig. 2 shows several characteristic vibrational modes confirming the presence of functional groups and lattice interactions. The asymmetric stretching of the carboxylate (COO^-) group was observed in the region of 1550–1640 cm^{-1}. The O-H stretching vibration that highlights the presence of hydroxyl groups was appeared as a broad absorption band in the 3400–3600 cm^{-1}. The C-H stretching vibrations of the acetate methyl group were observed at 2926 cm^{-1}. The bending vibration of the O–H bond was at 1385 cm^{-1}. Si-O-Si asymmetric stretching was observed at 1112 cm^{-1}. (McMillan, 1984; Pisciella and Pelino, 2005; Ellerbrock *et al.* 2024). A strong band at 866 cm^{-1} is due to Mo-O-Mo stretching vibrations, which confirm the orthorhombic structure. Additionally, a peak at 766 cm^{-1} corresponds to the stretching vibration influenced by Er–O coordination, while the band at 604 cm^{-1} is attributed to Er–O–Er lattice vibrations (Li *et al.* 2023) The presence of a low-frequency band in the region of 450–500 cm^{-1} further confirms the Si–O tetrahedral bending mode (Varkentina *et al.* 2015; Liu et al. 2020; Vogel *et al.* 2016).

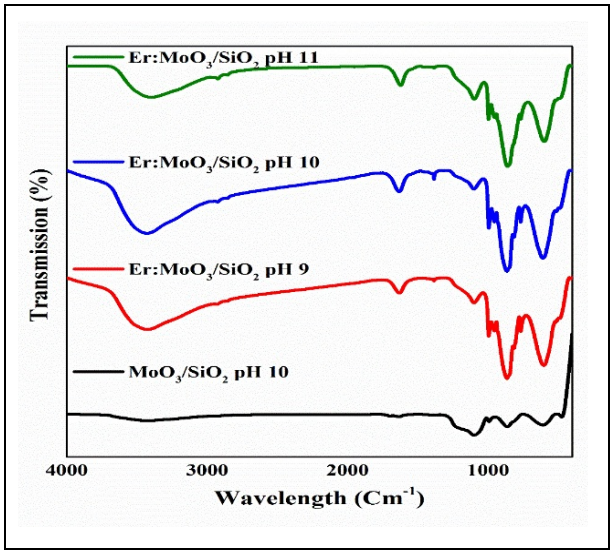


Fig. 2: FTIR Spectra of Er-doped MoO_3/SiO_2 nanoparticles at different pH

3.3 Raman Spectroscopy

Raman spectroscopy is an influential tool to analyze the quantum confinement effect, structural evolution of nanoparticles and its oxides. Raman spectra

for the samples (MoO_3/SiO_2 and $Er:MoO_3/SiO_2$ at different pH showed prominent change in bands attributed to the incorporation of dopant Er ions and the influence of pH. The peaks observed at 133, 163, 294, 333 cm^{-1} for MoO_3/SiO_2 were due to the Mo-O bending mode (Fig. 3). These peaks were found to decrease in Er: MoO_3/SiO_2 at pH 9, 10, and 11, which emphasizes replacement of bigger erbium ions in the lattice of molybdenum ions. New bands appeared at 400-750 cm^{-1} in $Er:MoO_3/SiO_2$ at pH 9, 10, and 11, affirming Si-O-Si bending/stretching (Nieto *et al.* 2024). Two nearby peaks in the range of 425-462 cm^{-1} were observed in $Er:MoO_3/SiO_2$ at pH 9, 10, and 11, which can be attributed to disordered silicates or mixed silica networks i.e., misfit dislocation of erbium ions within molybdenum matrix (Galeener, 1979; McMillan, 1984). Therefore, at higher pH (9 to 11) Er^{3+} ions replace Mo and Er-O, Er-O-Er. The bands observed between 520-600 cm^{-1} range show high energy symmetric and asymmetric M-O stretching or combination phonon in oxides. The increase in alkalinity in the prepared samples was observed in the Raman spectra. The peak shifts notably around 500-600 cm^{-1} and sharp peak at 526 cm^{-1} in $Er:MoO_3/SiO_2$ at pH 10 attributes to the moderate local distortion whereas, in $Er:MoO_3/SiO_2$ at pH 11 the peak appears broader. This analysis suggests that the moderate change in the pH enhances the crystallinity and low distortion in the lattice arrangement (Dieterle and Mestl, 2002).

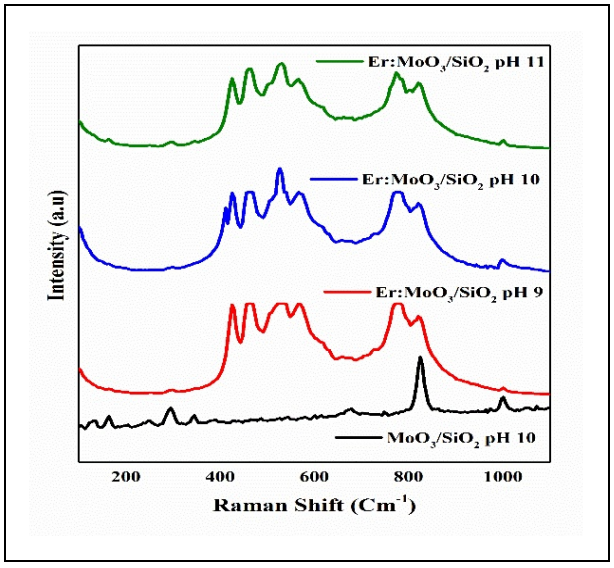


Fig. 3: Raman spectra of Er-doped MoO_3/SiO_2 nanoparticles at pH 9, 10 and 11

3.4 Photoluminescence Spectroscopy

The PL emission spectra of erbium-doped MoO_3/SiO_2 (pH 9, 10 and 11) nanoparticles were recorded by the excitation at 330 nm wavelength (Fig. 4). The presence of erbium was observed in the emission spectrum by several distinct transitions from visible to infra-red region 4 F 7/2 4 I 15/2 transition. Weak green emission appear in the region 520-550 nm corresponding to the 4 H 11/2 (Rashmi *et al.* 2021). Erbium replaces A-site cations or sits in defect associated sites near Mo-O clusters with oxygen vacancies, forming Er-O-Mo defect complexes that strongly influence luminescence (Rashmi *et al*. 2021; Liu *et al.* 2019; Hong *et al.* 2023). This is also confirmed in Raman spectroscopy. Erbium has lower charge, substitution of Mo requires charge compensation, and therefore erbium occupies interstitial voids localized near non-bridging oxygen. The increase in PL intensity at pH 9 suggests ideal contact between erbium ions and the lattice favoring radiative recombination. The silica matrix is stabilized at pH 9 whereas, structural distortion occurs at higher pH levels, such as the development of non-radiative recombination sites like defect clusters, oxygen vacancies, and Er-Er interactions leading to peak broadening. Therefore, at lower pH the luminescence behavior is improved and enhances the radiative transitions in the molybdenum host. pH 10 and 11 have high OH- that alter the local environment of erbium ions attributed to non-radiative decay (Pant *et al.* 2020).

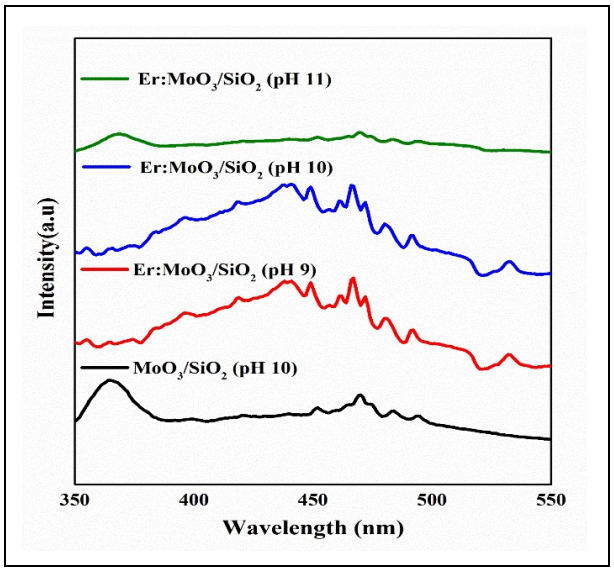


Fig. 4: Photoluminescence spectra of Er-doped MoO_3/SiO_2 nanoparticles at pH 9, 10 and 11

3.5 The EDAX Spectra

Fig. 5 demonstrates the successful incorporation of the Er dopant in MoO_3/SiO_2 with the prominent peaks of Mo, O, Er elements. The chemical purity of the sample was highlighted by the absence of redundant peaks.

The EDAX of Er-doped MoO_3 on SiO_2 reveals the elemental composition of the material, providing insight into the successful incorporation of erbium and other constituents. The spectrum revealed the following weight percentages: Mo (51.99%), O (36.65%) and Er (11.37%). These values confirm the stoichiometric nature of MoO_3 and the presence of Mo and O (Table 2).

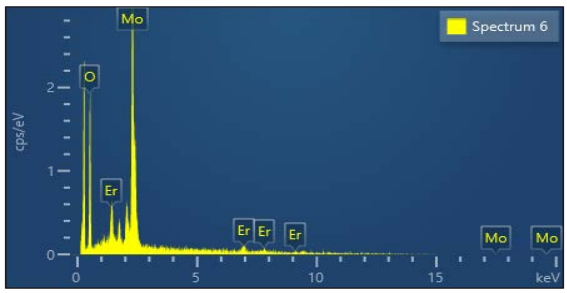


Fig. 5: EDAX Spectra of Er-doped MoO_3/SiO_2 nanoparticles at pH 9, 10 and 11

Table 2. Elemental composition of Er:MoO_3/SiO_2 nanoparticles

Element	Signal Type	Line	Wt%	Wt % Sigma	Atomic %
O	EDS	K series	36.65	1.42	78.97
Mo	EDS	L series	51.99	1.66	18.68
Er	EDS	L series	11.37	2.04	2.34
Total			100.00		100.00

Erbium, a rare earth dopant with notable optical and electronic properties, was found to constitute 11.37 wt% and 2.34 atomic%, indicating effective doping. Although its atomic percentage is relatively small compared to Mo and O, Er plays a decisive role as a functional additive. The obtained data suggest consistent elemental distribution. The minimum error indicates high reliability in the compositional analysis (Newbury, 2014; Scimeca *et al.* 2018; Duma *et al*. 2022; Garrido-García *et al*. 2024).

The EDAX spectrum accompanies the elemental composition, confirming the presence of Mo, O, Er and no impurities were detected. This alignment of structural and elemental data shows the successful integration of Er within the MoO_3/SiO_2. Dense agglomeration was seen in the morphology of Mo, O, Er particles. The obtained structure influences functional properties such as catalytic activity and absorption efficiency, making it suitable for various applications

3.6 FESEM Analysis

Shape, size and surface morphology of MoO_3/SiO_2 nanoparticles was demonstrated by FESEM. Fig. 6 shows the images of Er:MoO_3/SiO_2 nanoparticles of pH 9,10 and 11. It was observed that at pH 10 Er: MoO_3/SiO_2 nanoparticles had fine crystalline, uniform hexagon-like structure with a grain size about few nm. Image also shows irregular shaped structures leading to agglomeration. Similar agglomeration in MoO_3 nanoparticles was noticed by Chithambararaj *et al.* (2011). This confirms that in pH 10 the SiO_2 layer was coated well around the host material causing agglomeration whereas in pH 9 the structure of the host particle was clearly exposed.

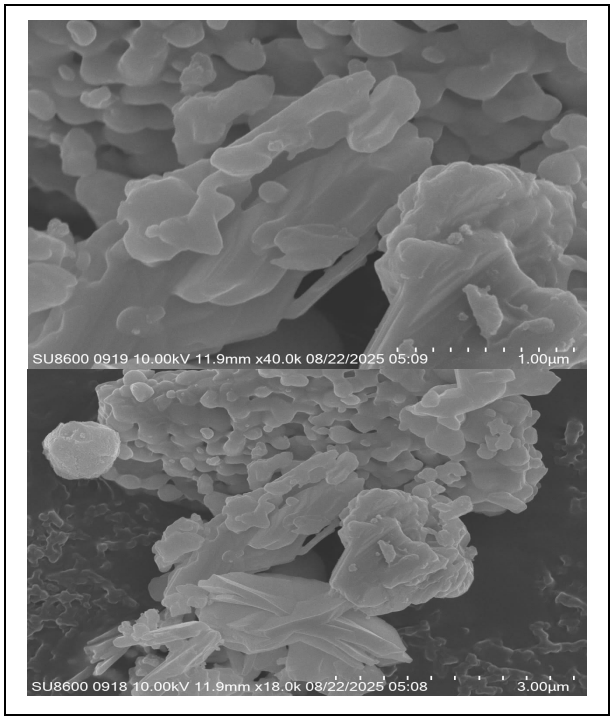


Fig. 6: FESEM image of Er doped MoO_3/SiO_2 nanoparticles at pH 10

4. CONCLUSION

The Er-doped MoO_3/SiO_2 nanoparticles were effectively synthesized by wet chemical method. The impact of change in pH in their structural and optical properties of the synthesized nanoparticles was examined by various characterization techniques. The change in pH did not bring out change in crystalline phase but it disturbed the crystallite size. The dopants occupy the interstitial sites in the host lattice. The chemical bonds were examined with FTIR analysis. The morphology of the synthesized samples was studied by typical FE-SEM image. Furthermore, the EDAX spectrum revealed the composition of the final compound and emphasizes that they are uniformly distributed throughout. The luminescent behavior of the nanoparticles studied by PL suggests that the material can find use in opto-electronic applications.

FUNDING

This research received no specific grant from any funding agency in the public, commercial, or not-for-profit sectors.

CONFLICTS OF INTEREST

The authors declare that there is no conflict of interest.

COPYRIGHT

This article is an open-access article distributed under the terms and conditions of the Creative Commons Attribution (CC BY) license (http://creativecommons.org/licenses/by/4.0/)

REFERENCES

Chithambararaj, A. and Bose, A.C., Hydrothermal synthesis of hexagonal and orthorhombic MoO_3 nanoparticles, *J. Alloys Compd*., 509(31), 8105-8110(2011). https://doi.org/10.1016/j.jallcom.2011.05.067

Chithambararaj, A., & Bose, A. C. (2011). Hydrothermal synthesis of hexagonal and orthorhombic MoO_3 nanoparticles. *Journal of Alloys and Compounds, 509*(31), 8105–8110. https://doi.org/10.1016/j.jallcom.2011.05.067

Danks, A. E., Hall, S. R. and Schnepp, Z., The evolution of sol–gel chemistry as a technique for materials synthesis. *Materials Horizons, 3*(2), 91–112 (2016). https://doi.org/10.1039/C5MH00260E

Dieterle, M. and Mestl, G., Raman spectroscopy of molybdenum oxides, *PCCP, 4*(5), 822–826 (2002). https://doi.org/10.1039/B107046K

Duma, Z. S., Tuomas, S., Jouni, H., Ville, R. and Satu-Pia R., Optimizing energy dispersive X-ray spectroscopy workflows for quantitative analysis, *Microchem. J.,* 180, 107685 (2022). https://doi.org/10.1016/j.micron.2022.103361

Ellerbrock, R. H., Stein, M. and Schaller, J., Comparing silicon mineral species of different crystallinity via FTIR, *Front. Environ. Chem.,* 4, 1462678 (2024). https://doi.org/10.3389/fenvc.2024.1462678

Galeener, F. L., Band limits and vibrational spectra of glass, *Phys. Rev. B, 19*(8), 4292–4297 (1979). https://doi.org/10.1103/PhysRevB.19.4292

Garrido-García, L. F., Pérez-Martínez, A. L., Reyes-Gasga, J., Aguilar-Del-Valle, M. D. P., Wong, Y. H. and Rodríguez-Gómez, A., A proof of principle using conventional EDX detectors for thin-film quantification, *Micromachines, 7*(3), 85 (2024). https://doi.org/10.3390/ceramics7030085

Hong, J., Liu, F., Dramićanin, M. D., Zhou, L. and Wu, M., Upconversion luminescence of Er^{3+}-doped $Ca_3Sc_2Si_3O_{12}$, *Nanomater.,* 13(12), 2071 (2023). https://doi.org/10.3390/nano13131910

Li, Y., Yu, S., Xiang, J., Zhang, F., Jiang, A., Duan, Y., Tang, C., Cao, Y., Guo, H. and Ying, Z., Revealing the Importance of Hole Transfer: Boosting Photocatalytic Hydrogen Evolution by Delicate Modulation of Photogenerated Holes, *ACS Catal.,* 13(12), 8281–92(2023). https://doi.org/10.1021/acscatal.3c01210

Liu, C., Quanlin, W., Xiao, W., Baisheng, S., Hailing, S., Laihui, L., Cong, L., Xinghua, Z., Tengfei, L., and Zhimei S., Upconversion dynamics of Er^{3+} emissions, *ACS Omega,* 4(23), 20029–20038 (2019). https://doi.org/10.1021/acsomega.9b01391

Liu, H., Seung, H. H., Mengguo, R., Mahadevan, T., Timothy, M. G., Jincheng, D., Adri, C. T. V. D. and Seong, H. K., Correlating vibrational spectral features and structure of silicates, *J. Am. Ceram. Soc., 103*(12), 7030–7044 (2020). https://doi.org/10.1111/jace.17036

McMillan, P., Structural studies of silicate glasses and melts—applications of Raman spectroscopy, *Am. Mineral., 69*, 622–644 (1984).

Newbury, D. E. and Ritchie N. W., Performing elemental microanalysis with high accuracy and precision, *Microsc. Microanal.,* 20(6), 1648–1658 (2014). https://doi.org/10.1007/s10853-014-8685-2

Nieto, P. E., Negrete, A. S., Ochando, M. I., Vondracek, M., Galiana, B., Pelaez, R. J., Mate, B., Lopez, A. S. and Serna, R., Building Nanoplatelet α-MoO_3 Films: A HighQuality Crystal Anisotropic 2D Material for Integration, *Appl. Surf. Sci.,* 672, 160871(2024). https://doi.org/10.1016/j.apsusc.2024.160871

Nirmal, P. R. A., Biju, B. R., Joel, C., Hari, S. K. and Daniel, A. S., Systematic Analysis and the Effect of Mn Doping on Structural, Optical and Magnetic Properties of MoO_3 Nanoparticles, *Solid State Commun.,* 341, 114532(2022). https://doi.org/10.1016/j.ssc.2021.114532

Pant, A., et al. (2020). Solid-state laser refrigeration of Er-doped hosts: upconverted green/red assignments. *Optics Express, 28*(3), 3995–4011. https://doi.org/10.1364/OE.383306

Pisciella, P. and Pelino, M., FTIR of crystallisation in iron-rich glass, *J. Eur. Ceram. Soc., 25*(11), 1855–1861 (2005). https://doi.org/10.1016/j.jeurceramsoc.2004.06.012

Rashmi, B. N., Sujatha F. H., Ravikumar, C. R., Avinash, B., Gurushantha, K., Divakara, M. B., Santosh, M. S. and Veena, K., MoO_3 nanoparticles based electrodes as novel electrochemical sensors for the detection of H_2O_2, *Mater. Today: Proce.,* 46, 5931-5935(2021). https://doi.org/10.1016/j.matpr.2020.09.161

Rashmi, B. N., Sujatha F., Harlapur, C. R., Ravikumar, B., Avinash, K., Gurushantha, M. B., Divakara, M. S. and Santosh, K. V., MoO_3-based electrodes for H_2O_2 sensing, *Mater. Today Proc., 46*, 5931–5935 (2021). https://doi.org/10.1016/j.matpr.2020.09.161

Varkentina, N., Marc, D., Arnaud, R., Marc, R., Yannick, P. and Lionel, C., High repetition rate femtosecond laser irradiation of fused silica studied by Raman spectroscopy, *Opt. Mater. Express, 6*(1), 79–90 (2015). https://doi.org/10.1364/OME.6.000079

Vogel, H., Meyer-Jacob, C., Thöle, L., Lippold, J. A. and Jaccard, S. L., Quantification of biogenic silica by FTIR, *Limnol. Oceanogr. Methods,* 14(9), 586–597 (2016). https://doi.org/10.1002/lom3.10129

Yang, G., Honglei, Y., Zhang., Xueyao., lqbal., Kanwal., Feng., Fan., Ma., Qin, J., Yuan, J., Cai, F., Ma, Y. and Jiantai, Surfactant-free self-assembly to the synthesis of MoO_3 nanoparticles on mesoporous SiO_2 to form MoO_3/SiO_2 nanosphere networks with excellent oxidative desulfurization catalytic performance, *J. Hazard. Mater.,* 397, 122654 (2020). https://doi.org/10.1016/j.jhazmat.2020.122654